JOURNAL OF MATERIALS SCIENCE 15 (1980) 1939–1946

The effect of thermal history on the crystallization kinetics of a liquid-quenched metallic glass

Part 2

P. G. BOSWELL
Dental School, University of Queensland, Turbot Street, Brisbane 4000, Australia

The initial stage of the sequential two-stage crystallization of liquid-quenched $(Ni_{0.5}Pd_{0.5})_{82}P_{18}$ metallic glass involves the diffusion-controlled growth of MS-I′ microcrystals having a time-dependent nucleation rate. The apparent activation energy for the MS-I′ stage is about 30% smaller than the activation energy for viscous flow in the phase-separated melt. Using calorimetric differential thermal analysis it is shown that stabilization of the glass resulting from a decrease in the quench rate from $\sim 2 \times 10^7$ to $\sim 5 \times 10^3$ K sec^{-1} corresponds to a decrease in the initial nucleation rate and to a decrease in the rate of decay of the nucleation rate. The subsequent MS-II stage involves the nucleation and growth of cellular grains having needle-like, dendritic or spherultic morphologies depending on the crystallization temperature. Cellular growth is controlled by interfacial kinetics which scales as the shear viscosity of the initial phase-separated melt.

1. Introduction

In Part 1 [1] it was shown that the overall features of the crystallization kinetics of a liquid quenched $(Ni_{0.5}Pd_{0.5})_{82}P_{18}$ amorphous alloy at temperatures above T_g were influenced by the initial quench rate. The crystallization kinetics were monitored using calorimetric differential thermal analysis and it was found that separate Kissinger plots were obtained for the MS-I′ and MS-II crystallization stages in rod, ribbon and splat-quenched specimens.

Part 2 examines in detail the effect of the initial quench rate on the crystallization kinetics by using the continuous-heating DTA measurements to extract the kinetic parameters appearing in the Avrami equation for isothermal transformation. Comparisons between the parameters for each of the three types of specimens reveal systematic variations which can be rationalized in terms of existing models for structural relaxation and liquid-phase separation in NiPdP glasses.

2. Analysis of continuous heating kinetics

2.1. Activation energies

In analysing the crystallization kinetics for continuous (linear) heating conditions it will be convenient to employ several standard approaches. The theoretical basis for each of these approaches has been considered elsewhere [2–4] so it will only be necessary to summarize the most relevant aspects. The methods require that dx/dt, the crystallization rate under non-isothermal conditions, can be described in terms of separate functions, $f(x)$ and $g(T)$, of x and T. Hence

$$dx/dt = f(x)\,g(T). \quad (1)$$

An expression of this form can be obtained by differentiating the Avrami equation,

$$x = 1 - \exp(-Kt^n) \quad (2)$$

where K and n are constants, to give

$$\frac{dx}{dt} = \frac{\partial x}{\partial t}\bigg|_T + \frac{\partial x}{\partial T}\bigg|_t \frac{dT}{dt}$$

$$= nK^{1/n}(1-x)\,[1n(1-x)^{-1}]^{(n-1)/n}, \quad (3)$$

0022–2461/80/081939–08$02.80/0

where $\partial x/\partial T$ at constant time is taken to be zero. For those systems in which the rate function K, displays a Vogel–Fulcher temperature behaviour we have

$$K = K_0 \exp [-B/(T - T_0)] \quad (4)$$

where B and T_0 are constants. By replacing B by Q/R and by setting $T - T_0$ equal to θ, we have a generalized formalism

$$K = K_0 \exp (-Q/R\theta), \quad (5)$$

which for $T_0 = 0$ is equivalent to an Arrhenius rate constant. The parameters appearing in Equation 5 are Q, the activation energy and R, the gas constant. By substituting Equation 5 into Equation 3 and integrating it can be shown that [2, 3]

$$\ln (\theta_x{}^2/\beta) = Q/nR\theta_x + \ln \{Q[\ln (1-x)^{-1}]^{1/n}/n^2 K_0{}^{1/n} R\}, \quad (6)$$

where β is the linear heating rate and θ_x is the temperature corresponding to a fraction transformed x. Equation 6 forms the basis of the Kissinger method [5] whereby $\ln (\theta_x^2/\beta)$ is plotted as a function of θ_x^{-1} to give a straight line having a gradient Q/nR and an intercept $\ln \tau$.

The temperature θ_x appearing in Equation 6 can be evaluated by integrating the DTA peak to give the fraction transformed at any specified temperature. This integration should allow for the effect of a finite heat-transfer coefficient through the use of a calibration constant (see Part 1). Alternatively, following Kissinger [5], one can use characteristic temperatures for which x is independent of the heating rate. Of these temperatures, the most frequently used is θ_m, the temperature corresponding to the maximum rate of reaction. Another useful temperature is θ_d, the temperature at which the DTA trace is observed to deviate from its baseline. It was pointed out in Part 1 that θ_d can be rigorously defined as the temperature at which dx/dt attains a constant value given by the sensitivity of the analysis system. From Equations 1, 5 and 6 we have

$$\theta_x = \frac{h(x) \cdot f(x)\, Q\beta}{(dx/dt)\, n^2 R}^{1/2},$$

where $h(x)$ is equal to $[\ln (1-x)^{-1}]^{1/n}$. Hence

$$dx/dt \approx nK_0{}^{1/n} f(x) \times \exp \{-[Q(dx/dt)/R\beta h(x) \cdot f(x)]^{1/2}\}.$$

The solution of this equation in x and β can be shown to be only weakly dependent on β for small x so it is reasonable to assume that x at T_d (i.e. when dx/dt is a constant) is independent of β.

In using the multiple-scan Kissinger method for those situations in which T_0 is finite but unknown, it will be convenient to evaluate an apparent activation energy Q^a, given by the gradient of a $\ln (T_x{}^2/\beta)$ versus T_x^{-1} plot.

We note, however, that

$$B = d(\ln [\theta^2/\beta])/d\theta^{-1} = [d(\ln [T^2/\beta])/dT^{-1} - 2T_0\, T\theta^{-1}](\theta T^{-1})^2.$$

Thus

$$Q^a = BR\,(T\theta^{-1})^2 + 2RT_0\, T\theta^{-1}.$$

The effective activation energy, Q^e at a temperature T for a Vogel–Fulcher temperature behaviour is $BR\,(T\theta^{-1})^2$. Hence $Q^a \approx Q^e$ if

$$BR(T\theta^{-1})^2 \gg 2R\, T_0\, T\theta^{-1}$$

i.e.

$$B \gg 2\, T_0\, (T - T_0)/T. \quad (7)$$

In the case of NiPdP glasses [6] $B \gtrsim 10^3$ K, $T_0 \approx 400 \pm 100$ K and $T_g \approx 600$ K so condition 7 is satisfied at temperatures close to T_g and the gradient of the conventional Kissinger plot can be used to evaluate Q^e for these materials.

2.2. Time exponent, n

The time exponent n, appearing in the non-isothermal rate equation (Equation 3) can be estimated using Piloyan [7] and Sestak [8] plots. The former involves plotting $\ln (dx/dt)$ versus θ^{-1} and the gradient of the plot for small x yields Q/n. The Sestak procedure on the other hand, involves plotting $\ln [\ln (1-x)^{-1}]$ versus θ^{-1} and the gradient gives Q. If T^{-1} is used instead of θ^{-1} then the gradients yield effective activation energies, the ratio of which gives n for a particular heating rate.

3. Results

3.1. Activation energies

3.1.1. Glass transition

Following Chen [9], the effective activation energy Q_g, for structural relaxation at T_g can be obtained by plotting $\ln (T_g{}^2/\beta)$ versus T_g^{-1}. A Kissinger plot of this type is shown in Fig. 1 and it was derived using previously reported [10] T_g data for ribbon specimens. A straight line through the data points gives a Q_g value of 450 ± 20 kJ mol^{-1}. Fig. 2 compares this Q_g with Chen's [6] values for

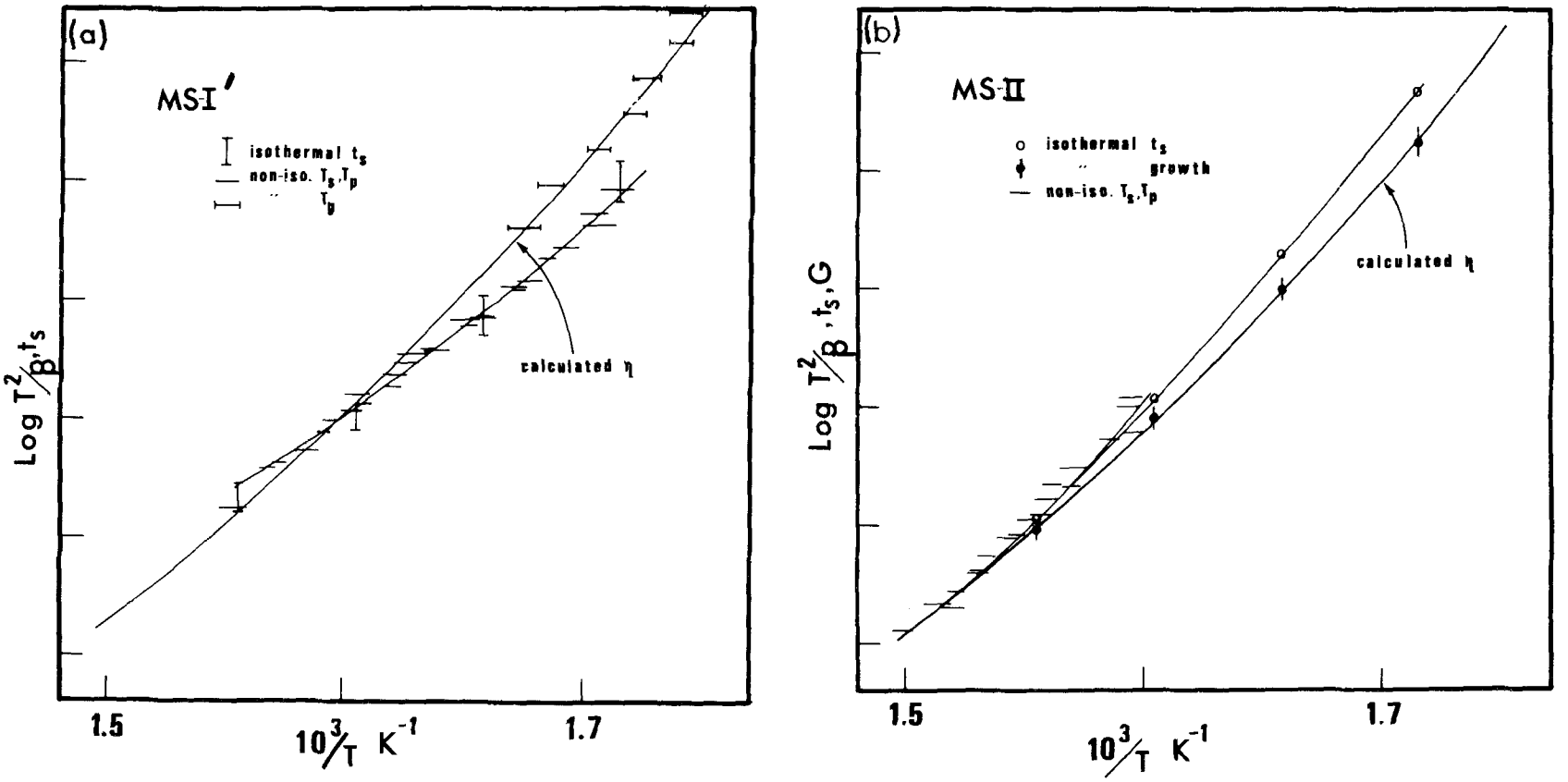

Figure 1 Time-constant adjusted, crystallization rate plots for the MS-I' and MS-II stages observed in heating a $(Ni_{0.5}Pd_{0.5})_{82}P_{18}$ amorphous alloy. T_g data are taken from [10] and the calculated viscosity curve is for $T_0 = 350$ K and $B = 8730$ K. The isothermal t_S and growth data are for ribbon specimens whereas the continuous-heating (Kissinger) data are for rod, ribbon and splat specimens.

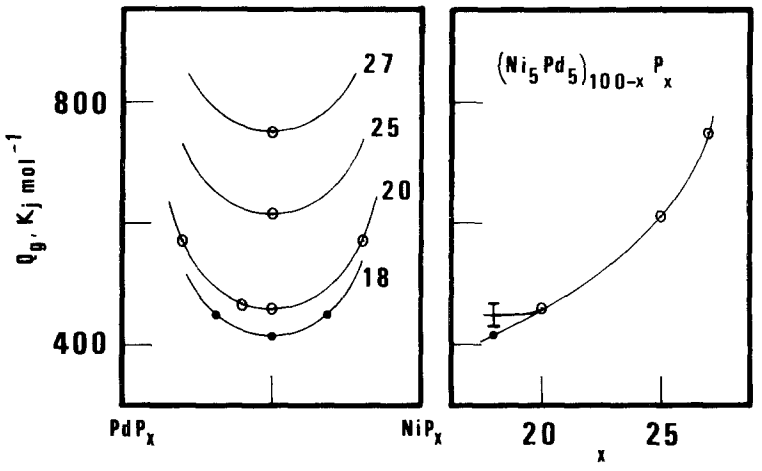

Figure 2 Composition dependence of Q_g, the average effective activation energy for viscous flow in Ni–Pd–P amorphous alloys. Data for alloys having $\geqslant 20$ at% P taken from [6].

$(Ni, Pd)_{100-x}P_x$ alloys having $x \geqslant 20$ and it can be seen that Q_g plateaus out for $(Ni_{0.5}Pd_{0.5})_{100-x}P_x$ alloys having $x \lesssim 20$. This behaviour is consistent with Chen's proposal [11] that alloys containing less than about 20 at% P phase separate in the liquid state to give two liquids having roughly the same P contents.

The composition dependence of the glass transition temperature for the P_{18} alloys can be described by drawing a curve through the observed Q_g value for the $(Ni_{0.5}Pd_{0.5})_{82}P_{18}$ alloy. Such is shown in Fig. 2 for $(Ni, Pd)_{82}P_{18}$ alloys. It was obtained by extrapolating the Q_g data to 18 at% P and then drawing a curve parallel to the Q_g data for $(Ni, Pd)_{80}P_{20}$ alloys. It can be seen that a Q_g of 450 kJ mol^{-1} requires that liquid-phase separation at invariant P yields two liquids having compositions of approximately $(Ni_{0.7}P_{0.3})_{82}P_{18}$ and $(Ni_{0.3}Pd_{0.7})_{82}P_{18}$. It is therefore envisaged that the thermally manifested T_g temperature in the $(Ni_{0.5}Pd_{0.5})_{82}P_{18}$ alloy was for both phase-separated liquids and that Q_g for these liquids was 450 ± 20 kJ mol^{-1}. Applying a construction similar to that for Q_g we find that Chen's T_0 and B data for NiPdP alloys gives $T_0 \approx 350$ K and $B \approx 8730$ K for the phase-separated melts. Fig. 1a shows that a curve calculated using these T_0 and B values appears to describe the slight temperature dependence of the T_g data for $(Ni_{0.5}Pd_{0.5})_{82}P_{18}$ with reasonable accuracy.

3.1.2. MS-I′ crystallization stage

The metallographically determined isothermal start times, t_s, for the MS-I stage (see Part 1) in ribbon specimens are plotted in Fig. 1a together with the Kissinger $\ln(T^2/\beta)$ plots for the non-isothermal MS-I′ stage. The data have been time shifted by displacing them along the vertical axis so that they superimpose upon a common curve. The average gradient of this curve yields an average effective activation energy of 300 ± 20 kJ mol^{-1} as compared with a calculated Q_g value of 410 ± 20 kJ mol^{-1}. This large difference between Q_g and Q (MS-I′) is graphically demonstrated in Fig. 1a showing that the kinetic data do not fall upon the calculated viscosity curve passing through the T_g measurements. It is therefore concluded that the MS-I crystallization kinetics did not scale as the shear viscosity of either component of the phase-separated melt; and that the MS-I′ kinetics in rod, ribbon and splat specimens can be rationalized in terms of progressive displacements along a common curve describing the temperature dependence of the crystallization kinetics.

3.1.3. MS-II crystallization stage

The metallographically determined MS-II growth rates (see Part 1) are plotted in Fig. 1b and it is evident that they fall upon the calculated viscosity curve if appropriate time-constant shifts are carried out. The MS-II growth rate therefore scaled as the shear viscosity. The metallographically determined MS-II t_S times (for ribbon specimens) are also plotted in Fig. 1b and it would appear that Q_S, the average effective activation energy for the MS-II start times was about 30 kJ mol^{-1} larger than Q_G the activation energy for MS-II growth. The start times included both nucleation and growth effects and according to the formal theory of transformation kinetics, $Q_S - Q_G \approx W^*/n$ where W^* is the activation energy for nucleation and n is the Avrami exponent. For MS-II reactions we would expect W^*/n to be about

10 kJ mol^{-1} and to be largely independent of temperature. The observed $Q_S - Q_G$ value appears to be significantly larger than the theoretical W^*/n which would indicate that different processes controlled nucleation and growth. A similar situation has been reported for an MS-II type crystallization reaction in an amorphous $Fe_{80}B_{20}$ alloy whereby $Q_S - Q_G$ was also estimated to be 30 kJ mol^{-1} [12].

The continuous-heating kinetic data for the MS-II stage (see Part 1) have also been plotted in Fig. 1b. There is reasonably good agreement between the temperature dependence of the isothermal t_S measurements for ribbons and of the continuous-heating data for rod, ribbon and splat specimens. The small difference between the average effective activation energies for these t_S and $\log(T^2/\beta)$ measurements can be attributed to the effect of self-heating of the specimen during crystallization at high heating rates. The effect of the initial quench rate on the activation energy for MS-II crystallization can therefore be interpreted in terms of displacement along a common curve. This curve displays an effective activation energy that is about 10% larger than the activation energy for viscous flow in the phase-separated melt because the continuous-heating measurements include both nucleation and growth effects.

3.2. Avrami parameters for the MS-I′ and MS-II stages

3.2.1. Time exponent, n

An example of the procedure for determining n, the exponent appearing in the Avrami rate equation, using Piloyan and Sestak plots has been presented elsewhere [2]. Fig. 3 gives the values obtained using the same procedure for the MS-I′ stage in the rod, ribbon and splat specimens. While the exponents for the rod specimens are somewhat scattered, it was nevertheless observed that n tended to decrease from ~ 1.8 to ~ 1.3 as the initial quench rate increased. There was also a trend towards an higher exponent as the heating rate increased. Hence, increasing the heating rate appeared to have the same effect as decreasing the initial quench rate.

While exponents measured during non-isothermal crystallization will, in general, not be equal to those measured during isothermal crystallization, they may nonetheless, approximate the isothermal exponents [3]. Moreover, differences

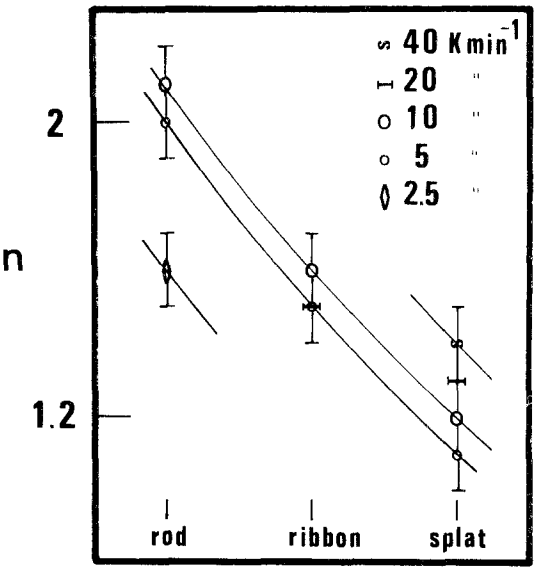

Figure 3 Quench-rate and heating-rate dependence of the time exponent n, appearing in the Avrami rate equation: MS-I′ crystallization stage under continuous-heating conditions.

between non-isothermal exponents may often be expected to parallel differences between isothermal exponents. It is therefore interesting to compare the experimentally determined n with theoretically predicted values. According to the formal theory of transformation kinetics (under isothermal conditions), $n = 5/2 + b$ for long-range diffusion controlled growth with a time dependent nucleation rate such that $I = I_0 t^b$ [13]. The observed decrease in n from ~ 1.8 to ~ 1.3 therefore indicates that b decreases from ~ -0.7 to ~ -1.2 as the quench rate increased. In other words, the non-isothermal kinetics data for the MS-I′ stage can be described in terms of long-range diffusion-controlled growth with a nucleation rate that decreased with time. Moreover, the rate of decrease of the nucleation rate increased as the quench rate increased or the heating rate increased.

3.2.2. Frequency factors

Proceeding with the interpretation of the effect of the initial quench rate in terms of displacement along common viscosity curves (see Fig. 1) we note that the time constant shifts which were required to give superimposed Kissinger plots varied systematically. The factors by which the Kissinger plots were multiplied by to give superimposition are plotted in Fig. 4 for the MS-I′ and MS-II stages. These factors are given by $\tau_{rod}/$

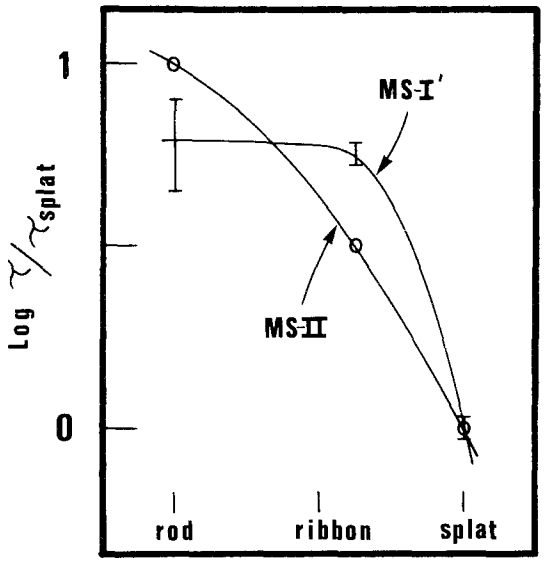

Figure 4 Quench-rate dependence of the intercepts of the Kissinger plots for the MS-I' and MS-II crystallization stages.

τ_{splat} and $\tau_{ribbon}/\tau_{splat}$ and it can be seen that they decreased as the quench rate increased.

In the analysis of the Kissinger method it was shown that $\tau \propto K_0^{-1/n}$. Also, in the formal theory of transformation kinetics for diffusion controlled reactions, $K_0^{1/n} \propto N$ where in the case of steady-state nucleation, N is equal to N_v the number atoms per unit volume for homogeneous nucleation; and to N_S the number of atoms in contact with nucleating substrates for heterogeneous nucleation. In the case of a zero nucleation rate, N becomes N_n the number of nuclei present at time zero. For the purpose at hand, the variation in $K_0^{1/n}$ and n for MS-I' upon increasing the quench rate can be modelled in terms of a time-dependent N such that

$$N = N_0 t^{-b}$$

where N_0 is the number of atoms that were initially able to take part in the nucleation of MS-I' microcrystals. According to this interpretation, the observed decrease in τ upon increasing the quench rate corresponds to an increase in N_0 from N_0 to $\sim 7N_0$ as the quench rate increased from rod to splat specimens. Thus, slowly quenched specimens were characterized by a relatively small number of atoms that initially took part in nucleation and a relatively slow rate of decrease in the number as MS-I' crystallization proceeded. Rapid quenches, on the other hand, increased the initial number of participating atoms but also increased that rate at which they became inactive.

With regard to the MS-II stage, it is noted that time exponents could not be measured because the MS-II crystallization exotherm for non-isothermal conditions overlapped with the transformation peak (see Part 1). However, the intercepts of the Kissinger plots decreased as the quench rate increased (see Fig. 4). Recalling that growth of the MS-II cells was found to be linear with time, and assuming $3 \leqslant n \leqslant 4$, it can be shown that τ is proportional to N_V^{-1}, N_S^{-1} or N_n^{-1} depending on the nucleation mechanism. Hence, increasing the quench rate tended to increase N_V, N_S or N_n for the MS-II stage.

4. Discussion

4.1. Activation energies

4.1.1. MS-I' crystallization stage

There have been several reports [14–16] showing that the apparent activation energies, Q, for an MS-I stage in a particular amorphous alloy are often smaller than the activation energies for the subsequent MS-II stage. However, none of this previous work related the activation energies for the MS-I and MS-II stages to the activation energy, Q_g, for viscous flow in the amorphous alloy (phase separated or otherwise). The results of the present investigation indicated that Q (MS-I') was smaller than Q_g even though liquid-phase separation probably preceded crystallization. Unfortunately, little is known about diffusion in metallic amorphous alloys near T_g. However, measurements of Au diffusivities in Pd–Si based amorphous alloys have indicated that any enhanced diffusion due to the retention of excess free volume is largely dissipated on continuous heating to temperatures above the thermally manifested T_g [17]. The relatively small activation energy for the MS-I' stage in the $(Ni_{0.5}Pd_{0.5})_{82}P_{18}$ alloy therefore cannot be ascribed to incomplete relaxation of the as-quenched glass. Instead, one is inclined to describe the MS-I' crystallization kinetics in terms of long-range diffusion control with an activation energy for solute diffusion that is smaller that the activation energy for viscous flow. Such a model requires that the undercooling required to drive the interfacial kinetic processes is but a small fraction of the total undercooling and this has been shown to be the case for MS-I' crystallites in $(Ni_{0.5}Pd_{0.5})_{82}P_{18}$ ribbons [2]. The model is also in accord with the measured time exponents of

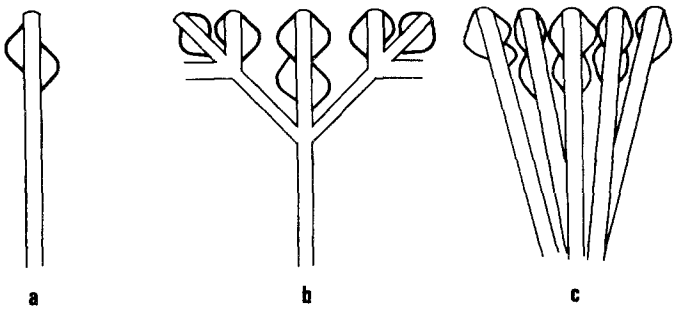

Figure 5 Schematic illustration of the transition from a needle-like MS-II growth at high temperatures to dendritic growth at intermediate temperatures and spherulitic growth at low temperatures. Growth in each case involves nucleation of a second phase on the phosphide constituent.

~ 1.3 to ~ 1.8 for the MS-I′ exotherm and with electron diffraction data for the MS-I stage in ribbon specimens. It was shown in Part 1 that the evolution of the MS-I crystallites from the amorphous matrix involved a progressive increase in the intensity of the MS-I electron diffraction rings as the fraction crystallized increased. It was argued that this behaviour could be attributed to the formation of an increasing amount of a cubic phase having roughly the same Ni and Pd content as the crystallizing phase-separated liquid but a lower P content. In other words, the electron diffraction data suggested that growth of the MS-I microcrystals involved solute segregation.

4.1.2. MS-II crystallization stage

In the case of the MS-II stage, it was established that the growth rate, the isothermal start times and the non-isothermal crystallization kinetics (if the effects of nucleation were allowed for), scaled as the viscosities of the phase-separated melts. It would therefore appear that the small amount of P redistribution that occured during the MS-I′ stage did not bring about a significant increase in the viscosity.

The TEM results reported in Part 1 showed that the MS-II growth morphologies varied from needle-like growth of the phosphide constituent at high temperatures to spherulitic growth at low temperatures: this transition in growth morphology is illustrated schematically in Fig. 5. Growth of the various MS-II structures involved growth of the phosphide with repeated epitaxial nucleation of a second phase. For needle-like morphologies the advancing tip of the phosphide needle "sees" an infinite matrix whereas for dendritic and spherultic morphologies, growth of the phosphide arms may be influenced by an array of overlapping diffusion fields. However, the MS-II growth rate scaled as the viscosity over the entire range of growth morphologies indicating that the growth of the MS-II grains was not affected by the composition profiles around isolated or arrayed phosphide arms. This would be the case if growth was controlled by interface kinetics and not by long-range diffusion. This conclusion is in agreement with calculations [2] showing that a large undercooling is required to drive the interfacial processes at the observed MS-II growth rates. Hence, while solute redistribution occured during MS-II growth, the growth rate was nonetheless controlled by interfacial diffusion which scaled as the shear viscosity of the phase-separated melt.

4.2. Effect of quench rate

Having established a reasonably consistent model for the crystallization behaviour of the $(Ni_{0.5}Pd_{0.5})_{82}P_{18}$ amorphous alloy, we now turn to the stabilization effect observed in decreasing the initial quench rate. Chen and Coleman [18] have suggested that the structural relaxation of liquid-quenched, metallic amorphous alloys involves localized relaxation at low temperatures and long-range co-operative relaxation at high temperatures. Localized relaxation is thought to produce atomic clusters which may act as embryos for MS-I′ nuclei [19, 20]. It is also likely that the clusters will tend to be broken up as a result of co-operative atomic movements at temperatures above T_g. The observed effect of clustering on MS-I′ crystallization kinetics might thus be expected to reflect a balance between the incorporation of clusters into critical nuclei and the annihilation of clusters. Chen and Coleman [18] also found that the intensity of structural relaxation increased as the quench rate increased. Accordingly, while higher quench rates favour the formation of a greater number of clusters they would also promote annihilation of the clusters during relaxation. This inference is in agreement with the results showing that increasing the quench rate increased both the number of atoms participating in nucleation and the rate at which these atoms were removed from the system.

Stabilization of the $(Ni_{0.5}Pd_{0.5})_{82}P_{18}$ alloy can therefore be interpreted in terms of the effects of structural relaxation during quenching on the nucleation kinetics of MS-I′ microcrystals during reheating.

4.3. Effects of the imposed heating conditions

It was found that increasing the linear heating rate increased the observed Avrami exponent, n (MS-I′), for a given initial quench rate. This behaviour can be attributed either to the effect of the heating rate on concentration gradients surrounding MS-I′ crystals or to its effect on structural relaxation. We note, however, that the characteristics of the relaxation spectra of metallic glasses are not strongly dependent on the heating rate [18] so we would not expect a large change in N_0 and b on increasing the heating rate. On the other hand, for diffusion-controlled growth, the Avrami exponent is a function of the heating rate [3]. The observation, in the present study, of such a functional dependence, albeit a relatively weak one, can therefore be construed as further support for the proposed interpretation of the MS-I′ crystallization kinetics.

5. Conclusions

The crystallization kinetics during the MS-I′ stage observed on heating a liquid-quenched $(Ni_{0.5}Pd_{0.5})_{82}P_{18}$ amorphous alloy can be interpreted in terms of long-range diffusion-controlled growth with a time-dependent nucleation rate. The activation energy for solute diffusion was about 30% smaller than the effective activation energy for viscous flow in the phase-separated melt.

Growth of the MS-II cellular crystallization product was controlled by interfacial kinetics which scaled as the viscosity of the phase-separated melt.

Stabilization of the glass resulting from a decrease in the initial quench rate corresponded to a decrease in the rate of decay of the nucleation rate and, more importantly, to a decrease in the number of atoms taking part in nucleation.

The effect of the quench rate on the nucleation rate of MS-I′ microcrystals can be interpreted in terms of competition between co-operative and localized relaxation during quenching and reheating.

References

1. P. G. BOSWELL, *J. Mater. Sci.* **15** (1980) 1926.
2. *Idem, Scripta Met.* **11** (1977) 701.
3. D. W. HENDERSON, *J. Non-Cryst. Solids* **30** (1979) 301.
4. T. OZAWA, *J. Thermal Analysis* **2** (1970) 301.
5. H. E. KISSINGER, *J. Res. Nat. Bur. Stand.* **57** (1956) 217.
6. H. S. CHEN, *J. Non-Cryst. Solids* **29** (1978) 223.
7. F. O. PILOYAN, I. O. RYABCHIKOV and O. S. NOVIKOVA, *Nature, London* **5067** (1966) 1229.
8. J. SESTAK, *Phys. Chem. Glasses* **6** (1974) 137.
9. H. S. CHEN, *J. Non-Cryst. Solids* **27** (1978) 257.
10. P. G. BOSWELL, *Scripta Met.* **11** (1977) 603.
11. H. S. CHEN, *Mat. Sci. Eng.* **23** (1976) 151.
12. U. KOSTER and U. HEROLD, *Scripta Met.* **12** (1978) 75.
13. J. BURKE, "The Kinetics of Phase Transformations" (Pergamon Press, Oxford, 1965).
14. C. P. P. CHOU and D. TURNBULL, *J. Non-Cryst. Solids* **18** (1975) 169.
15. M. A. MARCUS, *ibid.* **30** (1979) 317.
16. M. VON HEIMENDAHL and G. MAUSSNER, *J. Mater. Sci.* **14** (1979) 1238.
17. H. S. CHEN, L. C. KIMERLING, J. M. POATE and W. L. BROWN, *Appl. Phys. Letters* **37** (1978) 461.
18. H. S. CHEN and E. COLEMAN, *ibid.* **28** (1976) 245.
19. H. S. CHEN and S. Y. CHUANG, *ibid.* **31** (1977)
20. C. L. BRIANT, *Discuss. Faraday Soc.* **61** (1976) 25.

Received 3 August and accepted 5 December 1979.